Modification of the TSI 3081 differential mobility analyzer to include three monodisperse outlets

Comparison between experimental and theoretical performance

Bezantakos, S.; Giamarelou, M.; Huang, L.; Olfert, J.; Biskos, G.

DOI
10.1080/02786826.2016.1227060

Publication date
2016

Document Version
Final published version

Published in
Aerosol Science and Technology

Aerosol Science and Technology

ISSN: 0278-6826 (Print) 1521-7388 (Online) Journal homepage: http://www.tandfonline.com/loi/uast20

Modification of the TSI 3081 differential mobility analyzer to include three monodisperse outlets: Comparison between experimental and theoretical performance

S. Bezantakos, M. Giamarelou, L. Huang, J. Olfert & G. Biskos

To cite this article: S. Bezantakos, M. Giamarelou, L. Huang, J. Olfert & G. Biskos (2016) Modification of the TSI 3081 differential mobility analyzer to include three monodisperse outlets: Comparison between experimental and theoretical performance, Aerosol Science and Technology, 50:12, 1342-1351, DOI: 10.1080/02786826.2016.1227060

To link to this article: http://dx.doi.org/10.1080/02786826.2016.1227060

AEROSOL SCIENCE AND TECHNOLOGY
2016, VOL. 50, NO. 12, 1342–1351
http://dx.doi.org/10.1080/02786826.2016.1227060

Modification of the TSI 3081 differential mobility analyzer to include three monodisperse outlets: Comparison between experimental and theoretical performance

S. Bezantakos[a,b], M. Giamarelou[a], L. Huang[c], J. Olfert[d], and G. Biskos[b,c,e]

[a]Department of Environment, University of the Aegean, Mytilene, Greece; [b]Energy Environment and Water Research Center, The Cyprus Institute, Nicosia, Cyprus; [c]Faculty of Applied Sciences, Delft University of Technology, Delft, The Netherlands; [d]Department of Mechanical Engineering, University of Alberta, Edmonton, Alberta, Canada; [e]Faculty of Civil Engineering and Geosciences, Delft University of Technology, Delft, The Netherlands

ABSTRACT

Differential mobility analyzers (DMAs) are widely used to determine the size of aerosol particles, and to probe their size-dependent physicochemical properties when two are employed in tandem. A limitation of tandem DMA (TDMA) systems is their long measuring cycle when the properties of more than one monodisperse population of particles need to be probed. In this work, we propose a simple modification of the classical cylindrical DMA by including three monodisperse-particle outlets in its central electrode (namely, the 3MO-DMA), with the objective of using it as the first DMA in TDMA systems for reducing their measuring cycle. The performance of the 3MO-DMA at different flow conditions was evaluated using laboratory-generated aerosol particles, and compared with theoretical predictions. The theory predicted accurately (i.e., within 3%) the geometric mean diameters of the three distinct populations, as well as the resolutions of the first and the third outlet, under all experimental conditions. For the second outlet, the resolution was 10% to 74% lower than that predicted theoretically depending on the sheath-to-aerosol flow ratio. Nevertheless, the geometric standard deviation of the monodisperse aerosol from all the outlets was less than 1.09, which is sufficient for using the 3MO-DMA designed and tested in this work as a first DMA to produce a monodisperse aerosol flow containing three distinct particle populations in TDMA systems.

ARTICLE HISTORY
Received 7 June 2016
Accepted 15 August 2016

EDITOR
Kihong Park

1. Introduction

Particle size is a key parameter to understanding the processes through which atmospheric aerosols can affect human health and climate. The size of the particles in the breathing air, for instance, defines their deposition efficiency in our respiratory systems (Schlesinger 1985). In addition, it affects the ability of aerosols to scatter and absorb incoming solar radiation, which in turn defines the visibility and radiative properties of the atmosphere (Haywood and Boucher 2000). The size of atmospheric particles can also affect their ability to act as cloud condensation nuclei, thus changing the cloud properties and indirectly affecting climate at a local, regional, and global scale (Ogren and Charlson 1992). Measuring the variability in the size of atmospheric particles is therefore of primary importance for understanding their environmental impacts (McMurry 2000).

Early methods for sizing aerosol particles were based on size-dependent properties such as their diffusivity (for small particles) and inertia (for large particles). For example, diffusion batteries are used for classifying submicron particles (Cheng and Yeh 1980), while impactors (Marple 1970) and cyclones (Leith and Mehta 1973) are employed for segregating particles having sizes in the micron range. While simple and easy to construct, deploy, and maintain, these instruments exhibit limited resolution and measureable particle size range. The differential mobility analyzer (DMA; introduced by Hewitt 1957, and further developed by Knutson and Whitby 1975), on the other hand, provides a significant advantage in sizing resolution and extends the range of particle sizes that a single instrument can classify. DMAs, however, are more complex classifiers that exploit the motion of charged particles in a flowing aerosol under a well-

CONTACT G. Biskos g.biskos@tudelft.nl, g.biskos@cyi.ac.cy Energy Environment and Water Research Center, The Cyprus Institute, Nicosia 2121, Cyprus.

Color versions of one or more of the figures in the article can be found online at www.tandfonline.com/uast.
Supplemental data for this article can be accessed on the publisher's website.

defined electric field for determining their electrical mobility and thus their size.

Despite being more complex in design and construction than diffusion batteries and inertia classifiers, DMAs are the most effective tools for sizing aerosol particles. The most popular DMA design consists of two concentric cylindrical electrodes between which a high potential difference is applied to establish an electrostatic field. A particle-free sheath flow is introduced between the two electrodes, while charged polydisperse aerosol particles are introduced at the inner circumference of the outer cylindrical electrode. Depending on their electrical mobility, particles land at different positions along the inner electrode. Particles having electrical mobilities within a very narrow range exit the classifier through a monodisperse outlet slit located at a distance L downstream of the polydisperse aerosol inlet.

For a specific DMA design, the range of particle mobilities in the monodisperse flow depends on the operating conditions (i.e., flow rates and applied voltage between the two electrodes). The probability of particles coming through the inlet of the DMA to exit in the monodisperse flow under specific operating conditions is described by its transfer function. For large particles the transfer function can be derived from their deterministic trajectories inside the classification zone of the DMA (Knutson and Whitby 1975), whereas for smaller particles the effect of Brownian motion has to be taken into account (Stolzenburg 1988).

DMAs are employed in systems that measure the size distribution of particles by either step-increasing (Differential Mobility Particle Sizer, DMPS; Keady et al. 1983) or continuously scanning the potential difference between the two electrodes (Scanning Mobility Particle Sizer, SMPS; Wang and Flagan 1990). In addition, they are used in tandem (i.e., tandem DMA systems; Rader and McMurry 1986) for probing size-dependent properties of aerosol particles such as hygroscopicity (Bezantakos et al. 2013), volatility (Giamarelou et al. 2016), and charge probability (Biskos et al. 2005).

Several DMA designs have been proposed to cover a variety of requirements and applications. The classical, cylindrical, long DMA (TSI Model 3081 Long DMA), which was based on the design proposed by Knutson and Whitby (1975), can in principle classify particles having diameters down to ca. 5 nm. Increased particle diffusivity and losses on the walls, however, diminish their performance in terms of resolution and transmission for particles smaller than ca. 10 nm. To improve the resolution and reduce the diffusional losses of sub-10-nm particles, Chen et al. (1996; 1998) developed a short cylindrical DMA, which has also been commercialized by TSI (Model 3085 Nano DMA). Classification of sub-10-nm particles and atomic clusters with even higher resolution and transmission efficiency than that of the Nano DMA, have also been possible using high flow DMAs (de Juan and de la Mora 1998; Santos et al. 2009; Attoui et al. 2013; de la Mora and Kozlowski 2013; Maisser et al. 2015).

In contrast to the cylindrical design, radial DMAs that have been proposed in the 90s (Zhang et al. 1995; Mesbah et al. 1997) have higher penetration efficiency and resolution for particles ranging from 5 to 20 nm in size, and are typically more compact and portable. In an attempt to make DMAs even more portable and easier to build, Barmpounis et al. (2016) proposed new manufacturing methods (using mold casting or 3D printing) for building their main body out of polyurethane or other polymers, resulting also in a significant reduction in their manufacturing cost and weight without sacrificing the classification capabilities when compared to their metallic counterparts. Such DMAs can open the way for widespread use in monitoring using ground stations and airborne platforms such as balloons and drones, thereby providing adequate amount of spatially distributed measurements for better understanding the environment impacts of airborne particles.

With the objective to reduce the time needed for scanning over the different conditions to determine the size distributions of aerosol particles with SMPS or DMPS systems, Chen et al. (2007) designed and characterized a DMA with three monodisperse-particle outlets located along the outer cylinder. Results from that study were used to validate the theoretical transfer function for DMAs with multiple monodisperse outlets (i.e., MMO-DMA; Giamarelou et al. 2013). Apart from being used as a classifier in DMPS or SMPS systems, an MMO-DMA can also serve as a first DMA in TDMAs. The advantage of doing so is that it can allow simultaneous measurements of the properties of distinct monodisperse particle populations from the sampled polydisperse aerosol, thereby reducing significantly the measuring cycle of the system. Using the 3MO-DMA design proposed by Chen et al. (2007) (i.e., with the monodisperse outlet slits along the outer electrode) as the first DMA in TDMA configurations, however, would require the use of three single-monodisperse-outlet DMAs and an equal number of condensation particle counters (CPCs; Agarwal and Sem 1980) downstream each monodisperse-particle outlet, leading to an expensive and bulky system.

Here, we describe a simple modification of a classical cylindrical DMA (i.e., the TSI 3081 DMA) by including three monodisperse outlets along its central electrode. The resulting DMA (namely, the 3-monodisperse-outlet DMA; 3MO-DMA) yields a single aerosol flow including

three distinct populations of monodisperse particles, which makes it ideal for use as a first DMA in TDMA systems. The performance of the 3MO-DMA is tested under different operating conditions (i.e., flows and voltages) and compared with predictions using the transfer function provided by Giamarelou et al. (2012).

2. Experimental

2.1. Design of the 3MO-DMA

The 3MO-DMA described here was designed with the objective to use it as the first DMA (DMA-1) in a TDMA system. The classifier was a modified TSI 3081 DMA in which we replaced the inner electrode with one that includes three monodisperse-particle outlet slits. As a result, all three monodisperse particle populations were included in one flow, i.e., the monodisperse outlet flow of the TSI 3081. The position of each monodisperse slit along the inner electrode was selected so that particles classified through adjacent outlets differ in diameter by at least a factor two for the typical operating sheath flow rates (3–15 lpm) at a nominal pressure of 1 atm and temperature of 25°C. For example, when the 3MO-DMA is operated with a sheath flow of 3.0 lpm, an aerosol flow of 0.3 lpm, and a potential difference of 2 kV between the two electrodes, the midpoint mobility diameters of the particles classified through the outlets starting from the one closest to the inlet are 34.7, 99.8, and 248 nm (see the discussion further below). This feature is necessary for distinguishing particle populations of different hygroscopic properties as their size distributions measured by a second single-monodisperse-outlet DMA (i.e., DMA-2, operated at a scanning mode) will not overlap even if their hygroscopic growth factors are up to ca. 2 when exposed to typical operating relative humidity (RH) conditions of hygroscopic TDMA systems (i.e., in the range of 90%).

Figure 1 provides a schematic layout of the 3MO-DMA including the details of the inner electrode and the resulting particle size distributions upstream the inlet and downstream each of the three monodisperse-particle outlets. The top part of the inner electrode, which includes the sheath flow inlet, the threads for connecting the inner electrode to the main body of the DMA and the connection to the high voltage cable, was the same as that of the TSI 3081 Long DMA. The inner electrode was made out of a hollow tube having wall thickness of 3 mm and an outer radius of 10 mm (instead of 9.37 mm of the original TSI design). The three monodisperse outlet slits were located at 14.3, 95.0, and 397 mm downstream of the polydisperse aerosol inlet. These distances were determined by (Giamarelou et al. 2012)

$$L_i = \frac{(Q_{\mathrm{sh}_i} + Q_{\mathrm{m}_i})\ln\left(\frac{R_1}{R_2}\right)}{4\pi V Z^*_{\mathrm{p}_i}}, \qquad [1]$$

where R_1 and R_2 are, respectively, the inner and outer radii of the 3MO-DMA, V is the voltage of the inner electrode, whereas Q_{sh_i} is the sheath flow and Q_{m_i} is the excess flow

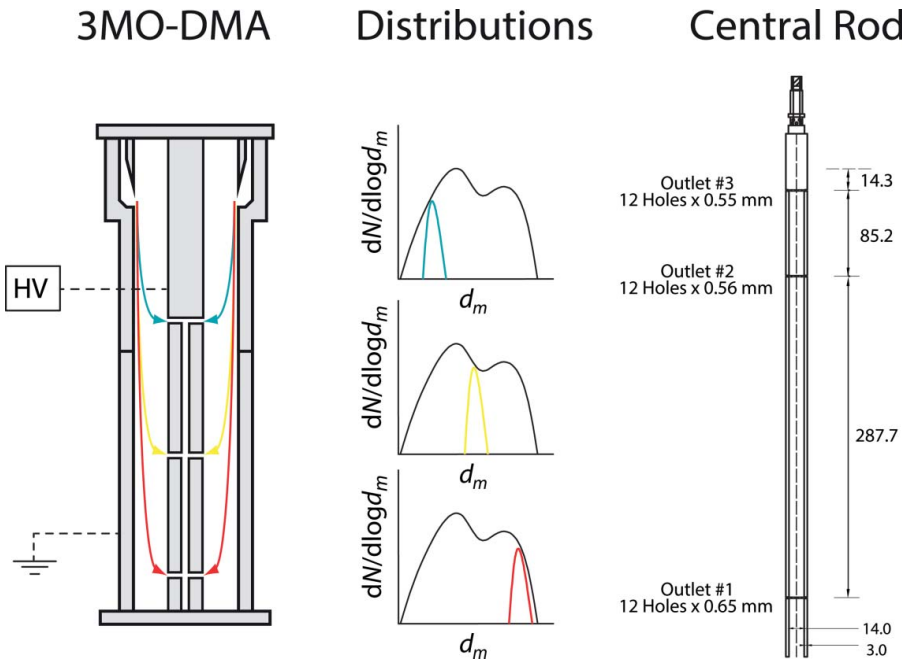

Figure 1. Schematic diagram of the 3MO-DMA, showing its operating principle and details of the design (see Table 1 for additional details).

of each monodisperse-particle outlet i given by

$$Q_{\mathrm{sh}_i} = \begin{cases} Q_{\mathrm{sh}} & \text{for } i = n \\ Q_{\mathrm{m}_{i+1}} - Q_{\mathrm{a}} & \text{for } 1 \le i \le n-1 \end{cases}, \quad [2]$$

and

$$Q_{\mathrm{m}_i} = \begin{cases} Q_{\mathrm{sh}} + Q_{\mathrm{a}} - Q_{\mathrm{s}_i} & \text{for } i = n \\ Q_{\mathrm{m}_{i+1}} - Q_{\mathrm{s}_i} & \text{for } 1 \le i \le n-1 \end{cases}. \quad [3]$$

Here n is the total number of monodisperse-particle outlets. Following the notation of Giamarelou et al. (2012), the numbering of the outlets starts from the one furthest from the polydisperse aerosol inlet (i.e., outlet 1 is the furthest while outlet #3 is the closest to the inlet). In the equations above, Q_{sh} and Q_{a} are, respectively, the initial sheath and aerosol flows (i.e., before entering the 3MO-DMA), while Q_{s_i} is the sample flow through each monodisperse-particle outlet i. In Equation (1), $Z^*_{\mathrm{p}_i}$ is the midpoint particle electrical mobility (i.e., the electrical mobility of the particles that start at the midpoint of the inlet and reach the midpoint of the outlet; Flagan 1999) classified through each outlet at a given set of operating conditions (i.e., flows and voltage). $Z^*_{\mathrm{p}_i}$ is associated with the midpoint particle mobility diameter $d^*_{\mathrm{p}i}$ through (Hinds 1999)

$$Z^*_{\mathrm{p}_i} = \frac{n_{\mathrm{e}} e C_c}{3\pi\eta d^*_{\mathrm{p}i}}. \quad [4]$$

Here, n_{e} and e are, respectively, the number of elementary charges the particles carry and the electron charge, whereas η is the air viscosity and C_c is the Cunningham slip correction factor (see supplementary information [SI] for details).

The flow rate through each monodisperse-particle outlet of the 3MO-DMA is determined by the total monodisperse flow pulled through the DMA, as well as the number and the diameter of the holes at each outlet through which particles pass from the classification region to the main monodisperse flow. Each outlet slit has 12 holes, the diameter of which were 0.55 mm for outlet #3, 0.56 mm for outlet #2, and 0.65 mm for outlet #1 (Figure 1). This allowed the sample flows through the outlets to progressively decrease when moving upstream, in order to minimize any potential flow disturbances caused by the proximity of outlets #3 and #2 (i.e., 14.3 and 95.0 mm, respectively) to the aerosol inlet. Using these dimensions, sample flow rates of approx. 26%, 33%, and 41% of the total monodisperse aerosol flow were estimated for outlets #3, #2, and #1, respectively.

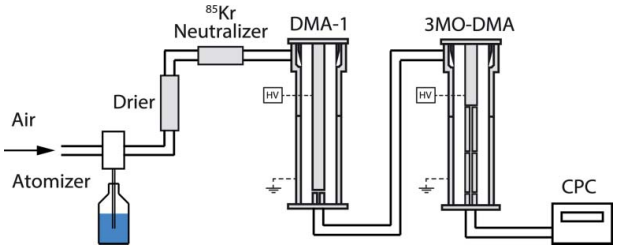

Figure 2. Experimental setup for determining the resolution of the 3MO-DMA at different operating conditions.

2.2. Characterization of the 3MO-DMA

2.2.1. Experimental setup

A tandem DMA system (Figure 2) was employed to determine the performance of the 3MO-DMA. In brief, polydisperse ammonium sulfate (AS) particles were produced by atomizing (with a TSI Model 3076 atomizer) a 0.1 w/v AS solution using N_2 (99% purity) as carrier gas. The resulting polydisperse aerosol, having particles smaller than ca. 500 nm, was dried to less than 10% RH using two silica gel diffusion driers in series, and charge neutralized by passing it through a ^{85}Kr aerosol neutralizer (TSI Model 3077). A custom-made single-monodisperse-outlet DMA (see Table 1 for its characteristic dimensions), employing a recirculating sheath flow system (see Biskos et al. 2006 for details) and a commercial high voltage (HV) power supply of negative polarity (Spellman V6A10N30), was used to provide a monodisperse aerosol flow. The mobility distributions of the monodisperse particles were then measured by the 3MO-DMA, employing the commercially available TSI 3080 recirculating sheath flow system and its built-in HV power supply that was coupled with an ultrafine Condensation Particle Counter (uCPC; TSI Model 3025; Stolzenburg and McMurry 1991). In all experiments, the voltage of the central electrode of the 3MO-DMA was stepwise increased with each step having a duration of 50 s. The average particle number concentration at each voltage was measured with the uCPC during the last 5 s of each step. The first 45 s were allowed for the concentration

Table 1. Characteristic dimensions of all the DMAs used in this work.

Type	Symbol	Description	Value	Unit
Custom single outlet DMA	L_c	Effective length	374.00	mm
	R_c	Outer radius	19.58	mm
	r_c	Inner radius	9.35	mm
TSI 3081 Long DMA	L_T	Effective length	443.69	mm
	R_T	Outer radius	19.61	mm
	r_T	Inner radius	9.37	mm
Custom 3MO-DMA	L_1	Effective length outlet #1	14.30	mm
	L_2	Effective length outlet #2	95.00	mm
	L_3	Effective length outlet #3	397.00	mm
	R_1	Outer radius	19.61	mm
	R_2	Inner radius	10.00	mm

to stabilize from that corresponding to the previous voltage settings.

The sheath and aerosol flows of both DMAs were measured before each experiment using a bubble flow meter (Sensidyne Gilibrator 2) in order to confirm that they were controlled within ±1% of their set-point values. Adequate drying (i.e., to less than 10% RH) of the polydisperse aerosol upstream the neutralizer was verified using a relative humidity and temperature sensor (Rotronic HC2-05). The operating voltages of both DMAs were frequently monitored to ensure that the HV power supplies were operating with a ±1% accuracy.

2.2.2. Data processing

Apart from the intrinsic properties of the sampled particles, the signals recorded by TDMA systems are predominantly defined by the size distribution of the sampled polydisperse aerosol, the transfer functions of the two DMAs employed, and the efficiency of the particle detector. Assuming that the number concentration of the polydisperse aerosol upstream DMA-1, the detection efficiency of the CPC and the particle losses in the tubing of the entire TDMA are constant, the response of the system can be expressed as (Li et al. 2006)

$$\frac{N_2}{N_1}=\frac{\int_0^{\infty}\Omega_1\left(Z_p,Z^*_{p_1}\right)\Omega_2\left(Z_p,Z^*_{p_2}\right)dZ_p}{\int_0^{\infty}\Omega_1\left(Z_p,Z^*_{p_1}\right)dZ_p}. \quad [5]$$

Here, N_1 and N_2 are, respectively, the particle number concentrations upstream and downstream of DMA-2; Ω_1 and Ω_2 are the transfer functions, whereas $Z^*_{p_1}$ and $Z^*_{p_2}$ are the electrical mobilities of particles reaching the midpoint of the outlet slit in DMA-1 and DMA-2, respectively. The theoretical transfer function of the cylindrical, single-monodisperse-outlet DMA (DMA-1 in this case) that takes into account the diffusivity of the particles is given by (Stolzenburg 1988)

$$\Omega_1\left(\tilde{Z}_{p_1}\right)=\frac{\sqrt{2}\sigma_1}{2\ \beta_1(1-\delta_1)}\left[\varepsilon\left(\frac{\tilde{Z}_{p_1}-(1+\beta_1)}{\sqrt{2\sigma_1}}\right)+\varepsilon\left(\frac{\tilde{Z}_{p_1}-(1-\beta_1)}{\sqrt{2\sigma_1}}\right)-\varepsilon\left(\frac{\tilde{Z}_{p_1}-(1+\delta_1\beta_1)}{\sqrt{2\sigma_1}}\right)-\varepsilon\left(\frac{\tilde{Z}_{p_1}-(1-\delta_1\beta_1)}{\sqrt{2\sigma_1}}\right)\right]. \quad [6]$$

Here $\tilde{Z}_{p_1}$ is the dimensionless particle electrical mobility ($Z_p/Z^*_{p_1}$), β_1 and δ_1 are the dimensionless flow parameters, and σ_1 is the dimensionless diffusional broadening parameter. Expressions of the above parameters and of function ε are provided in the SI. Equation (6) can be extended to predict the transfer function of DMAs with multiple monodisperse-particle outlets as follows (Giamarelou et al. 2012):

$$\Omega_{2_i}\left(\tilde{Z}_{p_{2_i}}\right)=\frac{\sqrt{2}\sigma_{2_i}}{2\ \beta_{2_i}(1-\delta_{2_i})}\left[\varepsilon\left(\frac{\tilde{Z}_{p_{2_i}}-(1+\beta_{2_i})}{\sqrt{2\sigma_{2_i}}}\right)+\varepsilon\left(\frac{\tilde{Z}_{p_{2_i}}-(1-\beta_{2_i})}{\sqrt{2\sigma_{2_i}}}\right)-\varepsilon\left(\frac{\tilde{Z}_{p_{2_i}}-(1+\delta_{2_i}\beta_{2_i})}{\sqrt{2\sigma_{2_i}}}\right)-\varepsilon\left(\frac{\tilde{Z}_{p_{2_i}}-(1-\delta_{2_i}\beta_{2_i})}{\sqrt{2\sigma_{2_i}}}\right)\right], \quad [7]$$

where i denotes the different monodisperse-particle outlets, which are numbered starting from the one furthest from the polydisperse aerosol inlet as discussed above.

Adjustable broadening parameters can be introduced in Equation (7) for treating disparities between theoretical and measured transfer functions, resulting in (Giamarelou et al. 2013)

$$\Omega'_{2_i}\left(\tilde{Z}_{p_{2_i}}\right)=\frac{\sqrt{2}\sigma'_{2_i}}{2\beta'_{2_i}\left(1-\delta'_{2_i}\right)}\left[\varepsilon\left(\frac{\tilde{Z}_{p_{2_i}}-\left(1+\beta'_{2_i}\right)}{\sqrt{2\sigma'_{2_i}}}\right)+\varepsilon\left(\frac{\tilde{Z}_{p_{2_i}}-\left(1-\beta'_{2_i}\right)}{\sqrt{2\sigma'_{2_i}}}\right)-\varepsilon\left(\frac{\tilde{Z}_{p_{2_i}}-\left(1+\delta'_{2_i}\beta'_{2_i}\right)}{\sqrt{2\sigma'_{2_i}}}\right)-\varepsilon\left(\frac{\tilde{Z}_{p_{2_i}}-\left(1-\delta'_{2_i}\beta'_{2_i}\right)}{\sqrt{2\sigma'_{2_i}}}\right)\right]. \quad [8]$$

The adjustable parameters β'_{2_i} and δ'_{2_i} here represent corrections in the flow rates (see the SI), while $\sigma'^2_{2_i}$ is the total adjusted spread parameter given by (Giamarelou et al. 2013)

$$\sigma'^2_{2_i}=f_{G_i}\sigma^2_{2_i}+\sigma^2_{mix_i}, \quad [9]$$

where $\sigma^2_{\mathrm{mix}_i}$ accounts for additional broadening of the transfer function caused by non-ideal mixing of the flows inside the MMO-DMA, while f_{G_i} is a factor accounting for any errors in estimating the unique geometric- and flow-condition-dependent parameter G_i (see the SI). The parameter $\sigma^2_{\mathrm{mix}_i}$, together with the adjusted flow parameters β'_{2_i} and δ'_{2_i}, determines the resolution in the non-diffusing limit, $R'_{nd_i}(\beta'_{2_i},\delta'_{2_i},\ \sigma^2_{\mathrm{mix}_i})$, which is defined

as the inverse of the normalized full-width at the half maximum (FWHM) value of the transfer function. Note that the theoretical (i.e., without using any broadening parameters) non-diffusing limit of the 3MO-DMA transfer function is given by (Giamarelou et al. 2013)

$$R_{nd_{2i}} = \frac{1}{\beta_{2_i}(1 + |\delta_{2_i}|)}. \quad [10]$$

The discrepancy between the theoretical and the measured/adjusted resolution can be expressed as

$$f_{Rnd_{2i}} = \frac{R'_{nd_{2i}}}{R_{nd_{2i}}}. \quad [11]$$

If the measured transfer function for a specific outlet i is broader than that predicted from theory, $R'_{nd_{2i}}$ will be smaller than $R_{nd_{2i}}$, and thus $f_{Rnd_{2i}}$ will be lower than unity.

The parameter f_{G_i} adjusts the asymptotic behavior of the 3MO-DMA resolution at the diffusing limit, which according to the theory (i.e., without using any broadening parameters) is given by (Giamarelou et al. 2013)

$$R_{diff_{2i}} = \frac{1}{2\sqrt{2\ln 2}}\frac{1}{\sigma^*_{2_i}} = \frac{1}{2\sqrt{2\ln 2}}\left[\frac{neV}{kTG_i \ln\left(\frac{R_1}{R_2}\right)}\right]^{1/2}. \quad [12]$$

Here, $\sigma^*_{2_i}$ is the total spread parameter of the transfer function of the ith outlet corresponding to a midpoint mobility diameter $Z^*_{p_i}$, k is the Boltzmann constant, and T is the absolute temperature. In a similar manner with Equation (11), a factor for comparing the measured with the theoretical resolution in the diffusing limit can be expressed as

$$f_{R\mathrm{diff}_{2_i}} = \frac{R'_{diff_{2i}}}{R_{\mathrm{diff}_{2_i}}}. \quad [13]$$

As with $f_{Rnd_{2i}}$, if the measured transfer function of the ith outlet is broader than that predicted by theory in the diffusing limit, $f_{R\mathrm{diff}_{2_i}}$ will be lower than unity.

Similarly to the comparison described in Giamarelou et al. (2013), a non-linear least-square fitting algorithm based on the interior-reflective Newton method (Coleman and Li 1994, 1996) was employed for comparing the measured response of the TDMA system with the theory (i.e., Equation (5)). The flow rates (i.e., sheath, excess, aerosol in and sample out flow rate), the pressure and temperature of both DMAs and the voltages of DMA-1, were allowed to vary within ±1% of the measured values, accounting for the associated experimental uncertainties. Larger variation (up to 30%) was allowed for the particle number concentrations upstream DMA-2 (i.e., N_1), to account for any instabilities in the particle generator. Diffusional losses of the sampled monodisperse particles inside the inner electrode of the 3MO-DMA were also taken into account as they affect the number concentration of the particles coming through each outlet. The total adjustable spread parameter of the transfer function $\sigma'^2_{2_i}$ was fitted once by varying f_{G_i} and once by modifying $\sigma^2_{\mathrm{mix}_i}$. The experimental resolution of the 3MO-DMA was expressed as the inverse of the FWHM of the fitted transfer function, normalized by the midpoint mobility of each outlet.

3. Results and discussion

The performance of the 3MO-DMA was evaluated at aerosol flow rates ranging from 0.3 to 1.5 lpm and sheath flow rates from 3.0 to 8.0 lpm (see Table 2 for more details) using DMA-classified particles of different sizes (see discussion below). The aerosol flow was controlled by the uCPC, whereas the sheath flow-rate was controlled by the sheath recirculating system as discussed above (Section 2.2.1).

Figure 3 shows an example of measured size distributions and corresponding predictions by Equation (5), using the theoretical 3MO-DMA transfer function without and with including the broadening parameters (i.e., using Equations (7) and (8), respectively). In the latter case, the fitting procedure was able to reproduce the observed mobility distributions with a normalized root mean square error (NRMSE) of less than 3% for the majority of the experimental data (i.e., 82% of the cases), whereas the maximum observed NRMSE (i.e., worst case of fitting) was ca.

Table 2. Ratio between measured and predicted resolutions of each outlet of the 3MO-DMA at the diffusive ($f_{R\mathrm{diff}_{2_i}}$) and the non-diffusive ($f_{Rnd_{2i}}$) limit, when operated at different flow conditions (Equations (11) and (13)).

Q_{sh} (lpm)	Q_a (lpm)	Outlet	$f_{R\mathrm{diff}_2}$	f_{Rnd_2}
3.0	0.3	3	1.00	0.991
		2	0.490	0.461
		1	0.987	0.981
6.0	0.6	3	—	0.984
		2	0.553	0.526
		1	1.05	0.997
8.0	0.3	3	0.992	0.978
		2	0.398	0.257
		1	0.939	0.970
8.0	1.5	3	—	0.998
		2	0.882	0.895
		1	0.987	0.996

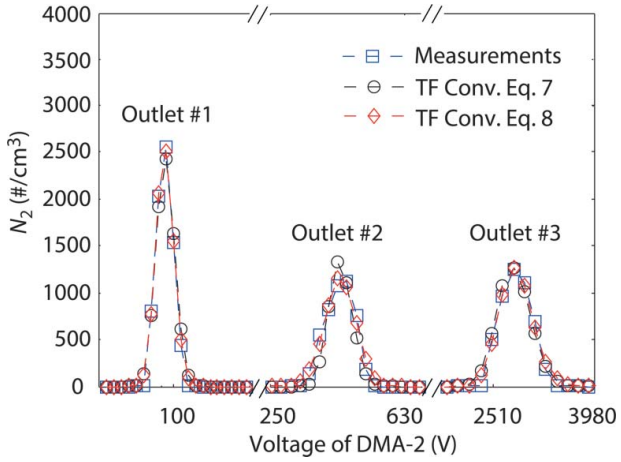

Figure 3. Measured and predicted (without and with considering broadening parameters, i.e., using Equations (7) and (8), respectively) response of the 3MO-DMA coupled with the CPC, when using 40-nm monodisperse ammonium sulfate particles.

6.2%. The fitted sample flow rates of each outlet corroborated our design calculations based on which 24% of the sample flow comes out of outlet #3, 33% out of outlet #2, and 43% out of outlet #1 (Section 2.1).

As shown in Figure 4, the fitting procedure (Section 2.2.2) reproduced the experimental results in terms of the midpoint mobility diameters within 3% accuracy in all the cases, even without using any broadening parameters. This suggests that for a fixed geometry and operating conditions, rearranging Equation (1) can be used to predict the midpoint electrical mobility for each outlet. It should be noted that agreement between predictions and measurements was similar in preliminary tests we did using the original central electrode of the TSI 3081 DMA (i.e., that with one monodisperse-particle outlet; data not shown), which corroborates findings reported earlier (Collins et al. 2004; Rodrigue et al. 2007).

Figure 5 shows the measured and predicted resolution without and with using the broadening parameters for each outlet of the 3MO-DMA. Table 2 also provides the median values of $f_{R\mathrm{diff}_{2_i}}$ and $f_{Rnd_{2i}}$ for each set of flow rates, determined by dividing the resolutions obtained from fitting the measurements to the calculations using theoretical transfer functions of DMA-1 and the 3MO-DMA at the diffusing and non-diffusing limits, respectively. Overall, as theory predicts, the measured resolution of each outlet increases as the sheath to

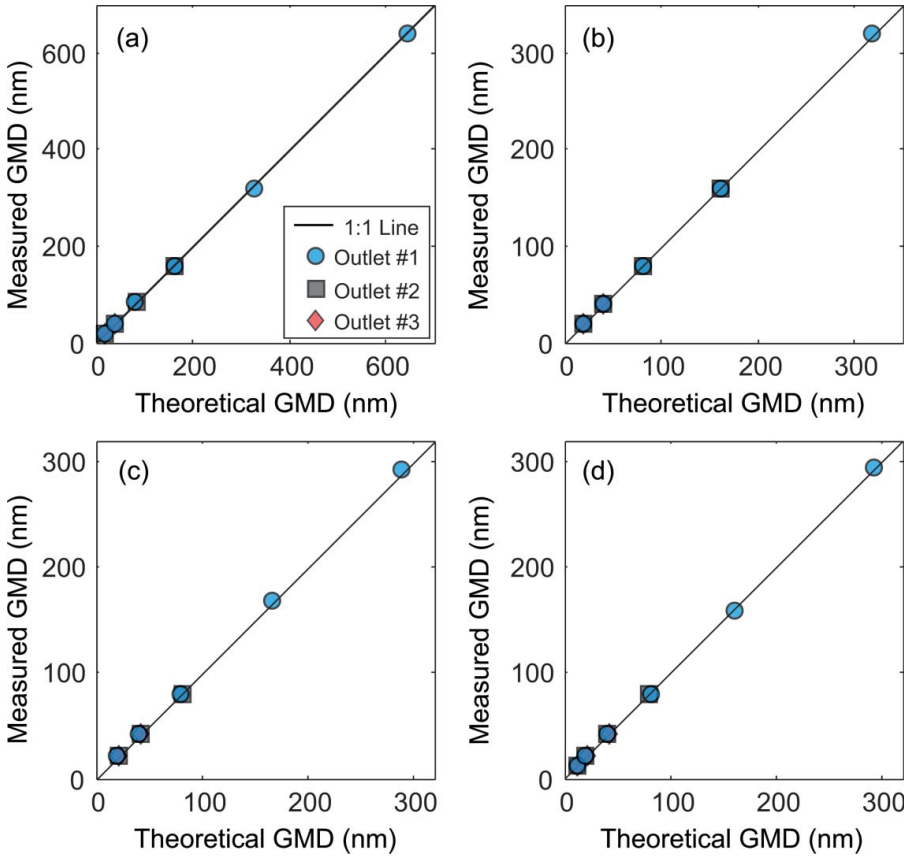

Figure 4. Measured vs. theoretically predicted geometrical mean diameters (GMD) of particles classified through each outlet of the 3MO-DMA, when operated with sheath to aerosol flow ratios of 3 lpm/0.3 lpm (a), 6 lpm/0.6 lpm (b), 8 lpm/0.3 lpm (c), and 8 lpm/1.5 lpm (d).

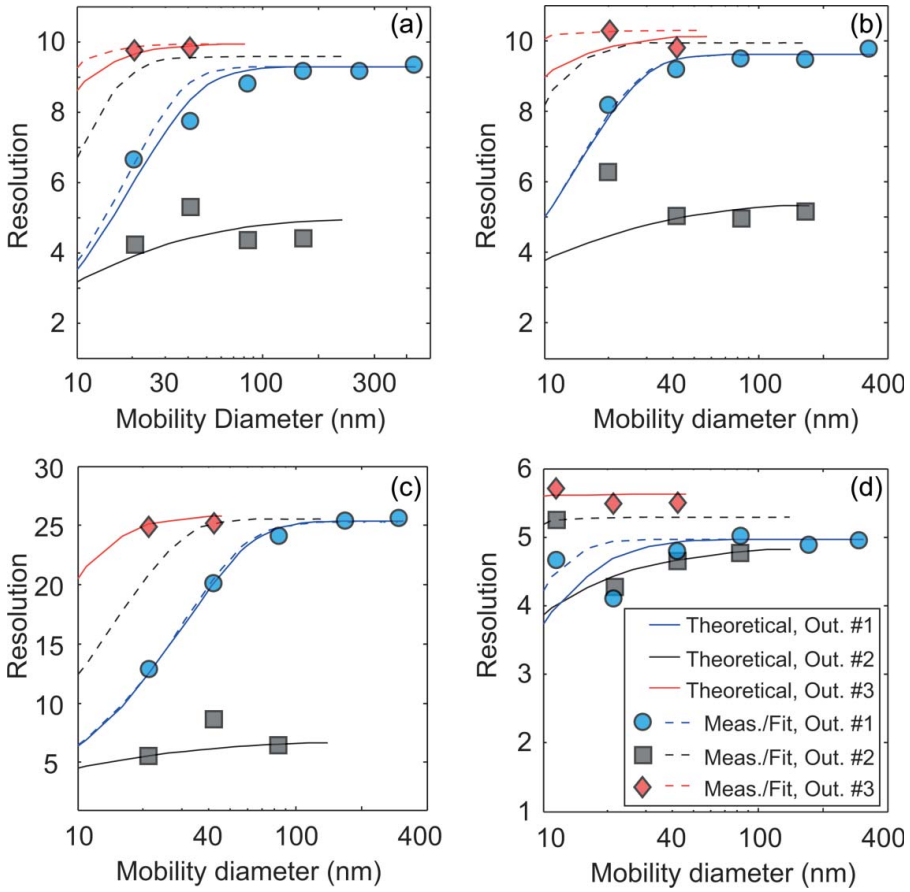

Figure 5. Resolution (1/FWHM) of each outlet of the 3MO-DMA, when operated with sheath-to-aerosol flow ratios of 3.0 lpm/0.3 lpm (a), 6.0 lpm/0.6 lpm (b), 8.0 lpm/0.3 lpm (c), and 8.0 lpm/1.5 lpm (d). The resolutions were estimated by convoluting the transfer functions of the DMAs used in the experimental setup (Figure 2), using fitted adjustable broadening parameters (i.e., f_{G_i} or $\sigma^2_{mix_i}$) for the 3MO-DMA transfer function (i.e., Equations (8) and (9)) to match the experimental size distributions (Section 2.2.2 and Figure 3). The theoretical resolutions (dashed lines) of each monodisperse outlet of the 3MO-DMA are determined using Equation (7). Fitted resolutions are determined by Equation (8) using the median values of the broadening parameters obtained from each data set (i.e., corresponding to the different sheath/aerosol flow rate ratios).

aerosol ratio increases. For outlets 1 (i.e., the one furthest from the aerosol inlet) and #3 (i.e., the one closest to the aerosol inlet), the ratios of the measured and the theoretical resolutions at the diffusing (i.e., $f_{R\mathrm{diff}_{2_i}}$) and at the non-diffusing limit (i.e., $f_{Rnd_{2i}}$) differ by less than 6% (Table 2). This indicates that under all tested flow conditions the theory can accurately predict the width of the transfer functions and thus the resolutions of these two 3MO-DMA outlets when particles of different sizes are classified.

In contrast, the measured resolution of outlet #2 differs significantly from that predicted theoretically. More specifically, when the 3MO-DMA is operated with a sheath to aerosol flow ratio of 10 (i.e., 3.0 or 6.0 lpm sheath flow, and, respectively, 0.3 or 0.6 lpm aerosol flow), the resolution of outlet #2 is reduced, compared to that predicted by theory, in the non-diffusing limit by ca. 50% (Table 2). At a sheath-to-aerosol flow ratio of 26.7 (i.e., 8.0 lpm sheath flow and 0.3 lpm aerosol flow), the measured resolution of outlet #2 deviates from predictions by almost 74%. Better agreement (i.e., within 12%) between measured and predicted resolution of outlet #2 was achieved when the 3MO-DMA was operated with a sheath-to-aerosol flow ratio of 5.33 (i.e., 8.0 lpm sheath flow and 1.5 lpm aerosol flow). Similar deviations were also observed at the diffusing limit.

As discussed above, the measured resolution of outlet #2 was significantly less than that predicted theoretically and even less than that of outlet #3 in all cases, which is also in contrast to what the theory predicts (Giamarelou et al. 2012). The fact that the measured resolution of outlet #2 is closer to the theoretical resolution when the 3MO-DMA was operated at the lowest sheath-to-aerosol flow ratio of 5.33 (i.e., sheath flow of 8 lpm and aerosol flow of 1.5 lpm; Figure 5d) suggests that the deviation is not a result of significant flow disturbances in the classification zone of the 3MO-DMA around the aerosol inlet and/or the outlets. This

indication was further corroborated by computation fluid dynamics (CFD) simulations (see the SI) and experiments during which outlet #3 was taped (data not shown here), both of which showed that the presence of outlet #3 does not affect the performance of outlet #2.

Despite the reduced resolution, the spread of the measured particle size distributions obtained from the middle outlet in terms of their geometric standard deviations (σ_g) was sufficiently monodisperse for TDMA measurements. Overall, the monodisperse samples obtained from the three outlets at all operated conditions had distributions with σ_g values smaller than 1.09. At the highest tested sheath-to-aerosol flow ratio (i.e., 26.7), for instance, the σ_g values obtained for outlets #1 and #3 were 1.03, while that obtained for outlet #2 was 1.05. At the lowest tested sheath-to-aerosol ratio (i.e., 5.33), the σ_g values were 1.09 for outlet #1, 1.08 for outlet #2, and 1.06 for outlet #3.

4. Conclusions

We designed, built, and tested a cylindrical DMA (namely, the 3MO-DMA) with the three monodisperse-particle outlets located on its central rod, which can be used as a first DMA in tandem DMA systems to reduce the time of the measuring cycle. The 3MO-DMA is a TSI 3081 DMA that was modified by replacing its central electrode with one containing three monodisperse-particle outlet slits. The locations of the outlets were selected so that size distributions of the three monodisperse particle populations are easily distinguishable when the DMA is operated at typical sheath flow rates.

The performance of the 3MO-DMA was tested at four different flow conditions using a tandem DMA configuration. The measurements were compared with predictions using the transfer function derived by Giamarelou et al. (2012). The results show that the theory can accurately (within 3%) predict the geometric mean diameter of the sampled particles for all the outlets. The experimental resolution (i.e., the inverse FWHM) of each outlet was estimated by fitting the theoretically predicted response of the system (Equation (5)) to the measurements, using adjustable broadening parameters for the diffusing and non-diffusing limits of the transfer function. Both measurements and predictions show that the resolution of each outlet increased with increasing sheath-to-aerosol flow ratio. The measured resolutions of the first and the third outlet were in good agreement with theoretical predictions (i.e., less than 6% difference). For the second outlet, however, measured resolutions were lower than those predicted by the theory. Excluding potential flow disturbances in the classification zone of the 3MO-DMA associated with the inlet and outlet flows, a possible explanation for this difference could be local distortions of the flow or the electric field that cannot be captured by the model. Higher deviations between measured and predicted resolution were observed at higher sheath-to-aerosol flow ratios. Despite these discrepancies, the geometric standard deviation of the size distributions of the particles classified through outlet #2 was not broader than 1.08, and can be considered monodisperse enough for tandem DMA measurements.

References

Agarwal, J. K., and Sem, G. J. (1980). Continuous Flow, Single-Particle-Counting Condensation Nucleus Counter. *J. Aerosol Sci.*, 11:343–357.

Attoui, M., Paragano, M., and de la Mora, J. F. (2013). Tandem DMA Generation of Strictly Monomobile 1–3.5 nm Particle Standards. *Aerosol Sci. Technol.*, 47:499–511.

Barmpounis, K., Maisser, A., Schmidt-Ott, A., and Biskos, G. (2016). Lightweight Differential Mobility Analyzers: Toward new and Inexpensive Manufacturing Methods. *Aerosol Sci. Technol.*, 50:2–5.

Bezantakos, S., Barmpounis, K., Giamarelou, M., Bossioli, E., Tombrou, M., Mihalopoulos, N., Eleftheriadis, K., Kalogiros, J., Allan, J. D., Bacak, A., Percival, C. J., Coe, H., and Biskos, G. (2013). Chemical Composition and Hygroscopic Properties of Aerosol Particles over the Aegean Sea. *Atmos. Chem. Phys.*, 13:11595–11608.

Biskos, G., Paulsen, D., Russell, L. M., Buseck, P. R., and Martin, S. T. (2006). Prompt Deliquescence and Efflorescence of Aerosol Nanoparticles. *Atmos. Chem. Phys.*, 6:4633–4642.

Biskos, G., Reavell, K., and Collings, N. (2005). Unipolar Diffusion Charging of Aerosol Particles in the Transition Regime. *J. Aerosol Sci.*, 36:247–265.

Cheng, Y. S., and Yeh, C. H. (1980). Theory of a Screen-Type Diffusion Battery. *J. Aerosol Sci.*, 11:313–320.

Chen, D., Pui, D. Y. H., Hummes, D., Fissan, H., Quant, F. R., and Sem, G. J. (1996). Nanometer Differential Mobility Analyzer (Nano-DMA): Design and Numerical Modeling. *J. Aerosol Sci.*, 27:S137–S138.

Chen, D., Pui, D. Y. H., Hummes, D., Fissan, H., Quant, F. R., and Sem, G. J. (1998). Design and Evaluation of a Nanometer Aerosol Differential Mobility Analyzer (Nano-DMA). *J. Aerosol Sci.*, 29:497–500.

Chen, D. R., Li, W., and Cheng, M. D. (2007). Development of a Multiple-Stage Differential Mobility Analyzer (MDMA). *Aerosol Sci. Technol.*, 41:217–230.

Coleman, T. F., and Li, Y. (1994). On the Convergence of Reflective Newton Methods for Large-Scale Nonlinear Minimization Subject to Bounds. *Math. Program.*, 67:189–224.

Coleman, T. F., and Li, Y. (1996). An Interior, Trust Region Approach for Nonlinear Minimization Subject to Bounds. *SIAM J. Optimiz.*, 6:418–445.

Collins, D. R., Cocker, D. R., Flagan, R. C., and Seinfeld, J. (2004). The Scanning DMA Transfer Function. *Aerosol Sci. Technol.*, 38:833–850.

De Juan, L., and de la Mora, J. F. (1998). High Resolution Size Analysis of Nanoparticles and Ions: Running a Vienna

DMA of Near Optimal Length at Reynolds Numbers up to 5000. *J. Aerosol Sci.*, 29:617–626.

De la Mora, F. J., and Kozlowski, J. (2013). Hand-Held Differential Mobility Analyzers of High Resolution for 1–30 nm Particles: Design and Fabrication Considerations. *J. Aerosol Sci.*, 57:45–53.

Flagan, R. C. (1999). On Differential Mobility Analyzer Resolution. *Aerosol Sci. Technol.*, 30(6):556–570.

Giamarelou, M., Stolzenburg, M., and Biskos, G. (2012). The Multiple Monodisperse Outlet Differential Mobility Analyzer: Derivation of its Transfer Function and Resolution. *Aerosol Sci. Technol.*, 46:951–965.

Giamarelou, M., Stolzenburg, M., Chen, D. R., and Biskos, G. (2013). Comparison Between the Theoretical and Experimental Performance of a Differential Mobility Analyzer with Three Monodisperse-Particle Outlets. *Aerosol Sci. Technol.*, 47:406–416.

Giamarelou, M., Eleftheriadis, K., Nyeki, S., Tunved, P., Torseth, K., and Biskos, G. (2016). Indirect Evidence of the Composition of Nucleation Mode Atmospheric Particles in the High Arctic. *J. Geophys. Res.-Atmos.*, 121:965–975.

Haywood, J., and Boucher, O. (2000). Estimates of the Direct and Indirect Radiative Forcing Due to Tropospheric Aerosols: A Review. *Rev. Geophys.*, 38:513–543.

Hewitt, G. W. (1957). The Charging of Small Particles for Electrostatic Precipitation. *Trans. Amer. Inst. Elect. Engr.*, 76:300–306.

Hinds, W. C. (1999). *Aerosol Technology: Properties, Behavior, and Measurement of Airborne Particles*. 2nd ed. John Willey & Sons, Inc., New York.

Keady, P. B., Quant, F. R., and Sem, G. J. (1983). Differential Mobility Particle Sizer: A New Instrument for High-Resolution Aerosol Size Distribution Measurement Below 1 μm. *TSI Quart.*, 9(2):3–11.

Knutson, E. O., and Whitby, K. T. (1975). Aerosol Classification by Electric Mobility: Apparatus, Theory, and Applications. *J. Aerosol Sci.*, 6:443–451.

Li, W., Li, L., and Chen, D. R. (2006). Technical Note: A New Deconvolution Scheme for the Retrieval of True DMA Transfer Function from Tandem DMA Data. *Aerosol Sci. Technol.*, 40:1052–1057.

Leith, D., and Mehta, D. (1973). Cyclone Performance and Design. *Atmos. Environ.*, 7:527–549.

Maisser, A., Barmpounis, K., Attoui, M. B., Biskos, G., and Schmidt-Ott, A. (2015). Atomic Cluster Generation with an Atmospheric Pressure Spark Discharge Generator. *Aerosol Sci. Technol.*, 49:886–894.

Marple, V. A. (1970). *A Fundamental Study of Inertial Impactors*, Ph.D. Dissertation, Department of Mechanical Engineering, University of Minnesota, Minneapolis, MN.

McMurry, P. H. (2000). A Review of Atmospheric Aerosol Measurements. *Atmos. Environ.*, 34:1959–1999.

Mesbah, B., Fitzgerald, B., Hopke, P. K., and Pourprix, M. (1997). A New Technique to Measure the Mobility Size of Ultrafine Radioactive Particles. *Aerosol Sci. Technol.*, 27:381–393.

Ogren, J., and Charlson, J. (1992). Implications for Models and Measurements of Chemical Inhomogeneities Among Cloud Droplets. *Tellus*, 44B:489–504.

Rader, D. J., and McMurry, P. H. (1986). Application of the Tandem Differential Mobility Analyzer to Studies of Droplet Growth or Evaporation. *J. Aerosol Sci.*, 17:771–787.

Rodrigue, J., Ranjan, M., Hopke, P. K., and Dhaniyala, S. (2007). Performance Comparison of Scanning Electrical Mobility Spectrometers. *Aerosol Sci. Technol.*, 41:360–368.

Santos, J. P., Hontañón, E., Ramiro, E., and Alonso, M. (2009). Performance Evaluation of a High Resolution Parallel-Plate Differential Mobility Analyzer. *Atmos. Chem. Phys.*, 9:2149–2429.

Schlesinger, R. B. (1985). Comparative Deposition of Inhaled Aerosols in Experimental Animals and Humans: A Review. *J. Toxicol. Environ. Health.*, 15(2):197–214.

Stolzenburg, M. (1988). *An Ultrafine Aerosol Size Distribution Measuring System*. Ph.D. Dissertation, University of Minnesota, St. Paul, MN.

Stolzenburg, M. R., and McMurry, P. H. (1991). An Ultrafine Aerosol Condensation Nucleus Counter. *Aerosol Sci. Technol.*, 14:48–65.

Wang, C. S., and Flagan, C. R. (1990). Scanning Electrical Mobility Spectrometer. *Aerosol Sci. Tech.*, 13:230–240.

Zhang, S. H., Akutsu, Y., Russell, L. M., Flagan, R. C., and Seinfeld, J. H. (1995). Radial Differential Mobility Analyzer. *Aerosol Sci. Tech.*, 23:357–372.